



Deformation-based morphometry identifies deep brain structures protected by ocrelizumab

Zhuang Song^{a,*}, Anithapriya Krishnan^a, Laura Gaetano^b, Nicholas J. Tustison^c, David Clayton^d, Alex de Crespigny^d, Thomas Bengtsson^a, Xiaoming Jia^e, Richard A.D. Carano^a

^a Personalized Healthcare Imaging, Genentech, Inc., South San Francisco, CA 94080, USA

^b Product Development Medical Affairs, F. Hoffmann-La Roche Ltd, CH-4070 Basel, Switzerland

^c Department of Radiology and Medical Imaging, University of Virginia, Charlottesville, VA 22904, USA

^d Clinical Imaging Group, Genentech, Inc., South San Francisco, CA 94080, USA

^e Biomarker Development, Genentech, Inc., South San Francisco, CA 94080, USA

ARTICLE INFO

Keywords:

Deformation-based morphometry
Brain atrophy
Multiple sclerosis
Biomarkers
Ocrelizumab

ABSTRACT

Background: Despite advancements in treatments for multiple sclerosis, insidious disease progression remains an area of unmet medical need, for which atrophy-based biomarkers may help better characterize the progressive biology.

Methods: We developed and applied a method of longitudinal deformation-based morphometry to provide voxel-level assessments of brain volume changes and identified brain regions that were significantly impacted by disease-modifying therapy.

Results: Using brain MRI data from two identically designed pivotal trials of relapsing multiple sclerosis (total $N = 1483$), we identified multiple deep brain regions, including the thalamus and brainstem, where volume loss over time was reduced by ocrelizumab ($p < 0.05$), a humanized anti-CD20 + monoclonal antibody approved for the treatment of multiple sclerosis. Additionally, identified brainstem shrinkage, as well as brain ventricle expansion, was associated with a greater risk for confirmed disability progression ($p < 0.05$).

Conclusions: The identification of deep brain structures has a strong implication for developing new biomarkers of brain atrophy reduction to advance drug development for multiple sclerosis, which has an increasing focus on targeting the progressive biology.

1. Introduction

Multiple sclerosis is an immune-mediated disorder of the central nervous system (CNS) and a leading cause of neurological disability in young adults. Multiple sclerosis is characterized by acute inflammatory disease activity leading to white matter demyelination and insidious progressive neurodegeneration, which results in neuroaxonal injury and accelerated grey matter atrophy (Compston and Coles, 2008; Miller et al., 2002). Grey matter atrophy may result from retrograde degeneration following focal white matter injury, but may also occur independently of white matter abnormalities (Calabrese et al., 2015).

Furthermore, grey matter atrophy occurs early in the disease course (Calabrese et al., 2007; Dalton et al., 2004; De Stefano et al., 2003), and shows greater correlation with clinical worsening than white matter changes (Fisniku et al., 2008). The availability of brain MRI in clinical practice and clinical trials enables systematic, non-invasive assessment of grey matter atrophy in the CNS.

Approved multiple sclerosis disease-modifying therapies (DMTs) generally reduce clinical relapses and acute disease activity in patients with relapsing multiple sclerosis (Sastre-Garriga et al., 2020; Vargas and Tyor, 2017); however, advanced biomarkers are needed to better assess their impact on disease progression, which may occur independent of

Abbreviations: 9HPT, Nine-Hole Peg Test; ANTs, advanced normalization tools; CDP, confirmed disability progression; CSF, cerebrospinal fluid; CNS, central nervous system; DBM, deformation-based morphometry; VBM, voxel-based morphometry; DMT, disease-modifying therapy; EDSS, Expanded Disability Status Scale; IFN, interferon; ITT, intention-to-treat; LME, linear mixed effects; OCR, ocrelizumab; ROI, region of interest; SST, single-subject template; T25FW, Timed 25-Foot Walk.

* Corresponding author at: Product Development - Personalized Healthcare Imaging, Genentech Inc., 1 DNA Way, South San Francisco, CA 94080, USA.

E-mail address: song.zhuang@gene.com (Z. Song).

<https://doi.org/10.1016/j.nicl.2022.102959>

Received 1 November 2021; Received in revised form 2 February 2022; Accepted 5 February 2022

Available online 14 February 2022

2213-1582/© 2022 The Author(s).

Published by Elsevier Inc.

This is an open access article under the CC BY-NC-ND license

(<http://creativecommons.org/licenses/by-nc-nd/4.0/>).

relapse activity and disproportionately affect long-term disability (Cree et al., 2019). Development of novel DMTs increasingly focus on targeting multiple sclerosis progressive biology, including reducing chronic focal inflammation and increasing neurorepair to halt neurodegeneration (Villoslada and Steinman, 2020). Therefore, sensitive and specific assessments of multiple-sclerosis-induced neurodegeneration, as well as novel atrophy-based biomarkers, are essential to facilitate development of therapies and advance care in multiple sclerosis.

Assessments of whole brain volume, while useful in some instances, does not fully capture the complexity of multiple sclerosis progressive biology (Calabrese et al., 2015) nor the hierarchically modular organization of the brain (Bullmore and Sporns, 2009). Instead, a localized assessment of brain atrophy may capture regional changes that are more specific to progressive biology, and thus may provide a better estimate of disease progression (Azevedo et al., 2018; Rocca et al., 2020). There is increasing evidence that spatial distribution of brain atrophy in multiple sclerosis is a non-random process (Haider et al., 2016; Steenwijk et al., 2016; Eshaghi et al., 2018a). Furthermore, spatial distribution of brain atrophy may change during the course of the disease and differ across clinical subtypes (Eshaghi et al., 2018a). It is therefore reasonable to hypothesize that the effects of DMTs on brain atrophy may also follow non-random spatial patterns across brain structures and thus more sophisticated methods are needed to quantify local brain atrophy. In addition, localized assessments of volume change may provide a more sensitive measure of treatment response. Nonetheless, early efforts of localized brain volume measurements in multiple sclerosis by using voxel-based morphometry (VBM) (Ashburner and Friston, 2000) have shown limited association with clinical outcomes (Lansley et al., 2013). As a result, whole brain volume change remains a standard assessment in multiple sclerosis clinical trials (Sastre-Garriga et al., 2020).

Measurement of localized brain volume changes may be affected by challenges in image registration and segmentation of brain regions and is further limited by the slow rate of multiple-sclerosis-related disease progression. Such errors can be minimized by methodology improvement and careful design of the longitudinal image processing pipeline. Of particular interest, deformation-based morphometry (DBM), which benefits from substantial improvements in image registration methods and does not necessarily rely on tissue segmentation or brain parcellation, in contrast to VBM or FreeSurfer (Fischl et al., 2004), has the potential to provide a precise voxel-level atrophy assessment (Chung et al., 2001; Manera et al., 2019).

This study aims to develop and apply a state-of-the-art longitudinal DBM methodology to provide voxel-level assessments of longitudinal brain volume changes, and to identify multiple sclerosis brain regions that are preferentially protected from volume loss following treatment with ocrelizumab (OCR). OCR is a humanized anti-CD20 + monoclonal antibody approved for the treatment of relapsing and primary progressive forms of multiple sclerosis, and significantly reduces brain atrophy and long-term disability in both populations (Hauser et al., 2017a; Montalban et al., 2017; Hauser et al., 2020; Wolinsky et al., 2020). Without restriction from predefined anatomical boundaries, the data-driven DBM method presented here was applied to identify unique spatial patterns of regional brain volume change that were associated with OCR treatment, and which may be associated with risk for confirmed disability progression. The DBM approach employed in this study exhibits great potential as a tool for future development of biomarkers of brain atrophy reduction for DMTs in multiple sclerosis.

2. Material and methods

2.1. Data

2.1.1. Patient population

This study was a retrospective analysis of two identically designed phase 3 clinical trials of relapsing multiple sclerosis (OPERA I: NCT01247324; OPERA II: NCT01412333). Details on patient selection,

MRI acquisition, and clinical assessments were provided in the original report (Hauser et al., 2017a). Briefly, patients were recruited with an age range of 18–55 years; 2010 revised McDonald criteria diagnosis of multiple sclerosis; Expanded Disability Status Scale (EDSS) score between 0 and 5.5; ≥ 2 documented clinical relapses within the previous 2 years or one clinical relapse within the year before screening; brain MRI evidence of multiple-sclerosis-related abnormalities. Patients were 1:1 randomized into two treatment groups: 1) OCR 600 mg every 24 weeks, or 2) interferon (IFN) β -1a 44 μ g three times per week throughout the 96-week treatment period. The intention-to-treat (ITT) population consisted of 1656 patients from OPERA I and II in total (821 in OPERA I; 835 in OPERA II). The minimum requirement for analysis of longitudinal changes in brain MRI data were that each patient must have brain MRI data available and successfully processed for the baseline and the first follow-up visit (Week 24). With this requirement, the patient sample size was reduced to 1483, with 742 in OPERA I and 741 in OPERA II. Demographic information and disease characteristics at baseline for this population are presented in Table 1, which were comparable to the ITT population as given in the original report (Hauser

Table 1
Demographic and disease characteristics at baseline of the study sample.

	OPERA I		OPERA II	
	Ocrelizumab (N = 375)	Interferon β -1a (N = 367)	Ocrelizumab (N = 374)	Interferon β -1a (N = 367)
Age, years, mean \pm SD	37.2 \pm 9.3	37.3 \pm 9.5	36.9 \pm 8.9	37.2 \pm 8.9
Female sex, n (%)	247 (65.9)	248 (67.6)	236 (66.5)	248 (67.6)
Time since symptom onset, years \pm SD	6.81 \pm 6.30	6.22 \pm 5.93	6.60 \pm 5.93	6.71 \pm 6.17
Time since diagnosis, years \pm SD	3.87 \pm 4.84	3.68 \pm 4.56	4.12 \pm 4.88	4.03 \pm 4.98
Relapses in previous 12 months, n \pm SD	1.30 \pm 0.66	1.34 \pm 0.65	1.34 \pm 0.69	1.35 \pm 0.75
EDSS score, mean \pm SD	2.79 \pm 1.22	2.72 \pm 1.27	2.74 \pm 1.30	2.75 \pm 1.38
No. of gadolinium-enhancing lesions on T1-weighted MRI, n/N (%)				
0	210/371 (56.6)	227/363 (62.5)	227/371 (61.2)	218/366 (59.6)
1	59/371 (15.9)	48/363 (13.2)	52/371 (14.0)	57/366 (15.6)
2	29/371 (7.8)	29/363 (8.0)	28/371 (7.5)	34/366 (9.3)
3	19/371 (5.1)	13/363 (3.6)	13/371 (3.5)	9/366 (2.5)
≥ 4	54/371 (14.5)	46/363 (12.6)	51/371 (13.7)	48/366 (13.1)
Lesions on T2- weighted MRI, n \pm SD	50.61 \pm 38.86	50.33 \pm 39.45	49.30 \pm 38.80	50.24 \pm 35.08
Volume of lesions on T2-weighted MRI, cm ³ \pm SD	11.01 \pm 14.13	9.48 \pm 11.06	10.56 \pm 13.67	10.48 \pm 12.31
Volume of lesions on unenanced T1-weighted MRI, cm ³ \pm SD	3.54 \pm 5.98	3.24 \pm 5.02	3.47 \pm 5.86	3.33 \pm 5.24
Normalized brain volume, cm ³ \pm SD	1499.26 \pm 83.80	1498.96 \pm 85.85	1503.66 \pm 91.58	1502.64 \pm 89.80

Abbreviations: EDSS, expanded disability status scale, SD: standard deviation.

et al., 2017a). In addition, study sample size per visit is shown in Table S1.

2.1.2. Imaging protocols

Conventional T1-weighted, 3D-spoiled, gradient-recalled echo brain MRI (before Gadolinium injection) was acquired at baseline, Weeks 24, 48, and 96 (repetition time = 28–30 ms, echo time = 5–11 ms, flip angle = 27–30 deg, 60 oblique axial slices of 1 mm in-plane resolution and 3 mm slice thickness without gap). For measuring lesion burden in white matter at every visit, the same T1-weighted brain MRI sequence was acquired after Gadolinium injection, in addition to conventional T2-weighted 2D multi-slice turbo/fast spin-echo and T2-weighted 2D Fluid-Attenuated Inversion Recovery (FLAIR), all of which were acquired with the same slice orientation and voxel size. Lesion burden was evaluated centrally at NeuroRx Research, Montreal, Quebec, Canada.

2.2. Longitudinal DBM pipeline

The longitudinal DBM pipeline used in this study is illustrated in Fig. 1. The main part of this pipeline was recently developed (Tustison et al., 2019) within the open source toolkit Advanced Normalization Tools (ANTs) (Avants et al., 2014). At its core, the diffeomorphic image registration method of ANTs has been developed and extensively

validated with human brain MRI data (Avants et al., 2011; Klein et al., 2009) and is widely recognized as a top performer of nonlinear image registration in neuroimaging research. The Mindboggle atlas (Klein and Tourville, 2012), which is a modification of the popular Desikan–Killiany–Tourville labelling protocol (Desikan et al., 2006), was used to identify individual brain structures.

Prior to individual patient data processing, a population-specific group template of the T1-weighted brain MRI was constructed by an unbiased, iterative method in ANTs (Avants et al., 2010), with T1-weighted brain MR images of 171 healthy adults (aged 20–59 years) from the Dallas Lifespan Brain Study (Park Aging Mind Laboratory), which had a similar age range as the patients in the OPERA studies. Before being fed into the pipeline, each individual brain image from the OPERA studies was preprocessed with the following steps: 1) resampling to an isotropic resolution of 1 mm; 2) N4 bias correction (Tustison et al., 2010); and 3) denoising with a non-local algorithm (Manjón et al., 2010).

Within each patient, a key step in the longitudinal DBM pipeline was to create a single-subject template (SST) from the images of all visits for each patient using the same image processing steps that were employed to create the population-specific group template. After the SST was generated, the spatial transformation between the SST and each individual image was used to create a voxel-wise map of the Jacobian

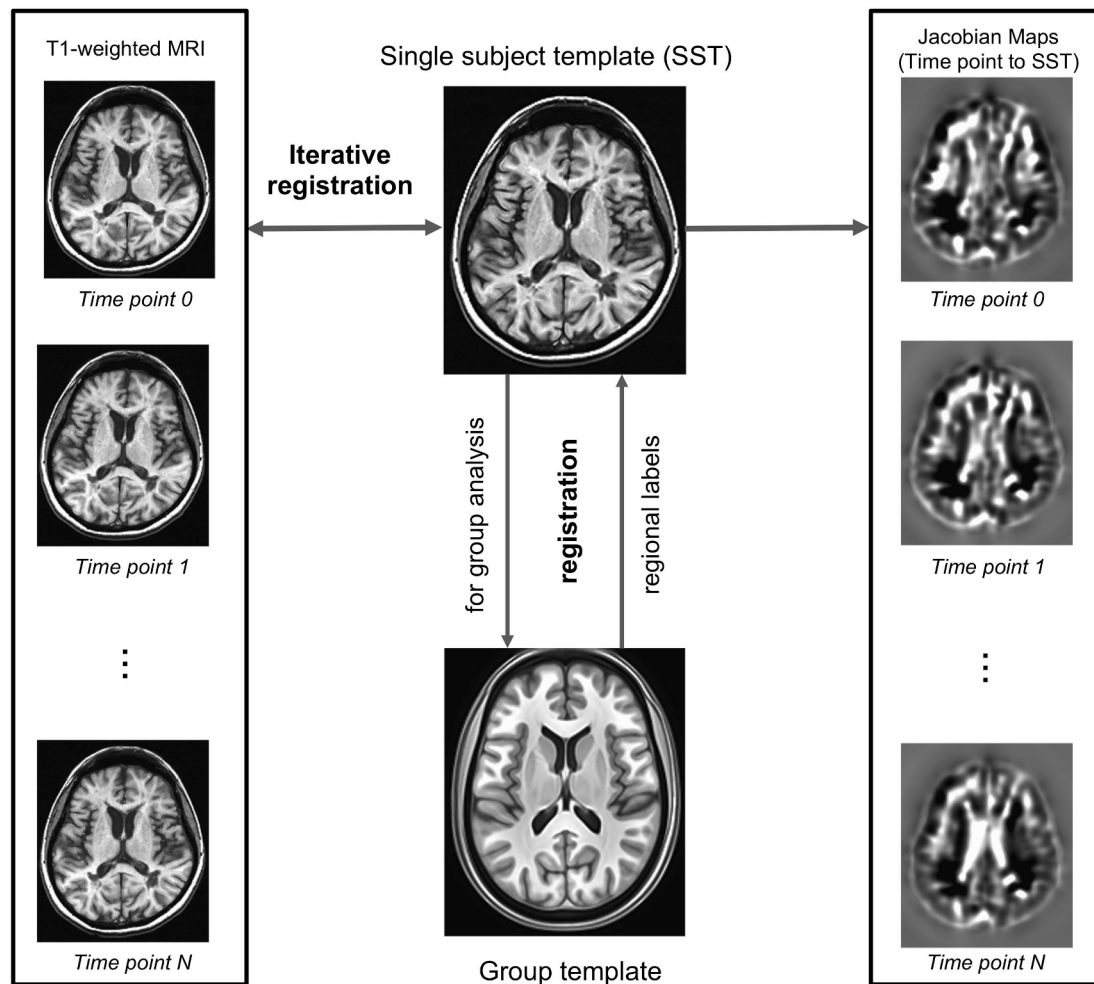


Fig. 1. Illustration of the longitudinal deformation-based morphometry pipeline. For each patient, a single-subject template (SST) is created with iterative registration from T1-weighted brain MRI of N time points, which is designed to be unbiased to any time point (left column). For each individual image, the registration with the SST of the same patient generates a Jacobian map over the whole brain (right column), which is a voxel-level measure of volume using the SST as the reference. A population-specific group template is created in a separate process. The spatial transformation from each SST to the group template allows the Jacobian maps in the SST space of each patient to be mapped into a common spatial coordinate of the brain in order to perform group-level voxel-wise analyses. Additionally, regional labels can be mapped from the group template to each SST in order to measure volume of regions of interest (ROIs) at the patient level.

determinant (also referred to as the Jacobian), which is a measure of voxel-level volume in each individual image (as a ratio to the volume of the same voxel location in the SST). Longitudinal volume change across time points at each voxel can be thus estimated as a change of the Jacobian value at the voxel location. The SSTs were then registered to the group template by ANTs. Once the spatial transformation was established, individual Jacobian maps in the SST space were transferred to the group template for group-level analysis. Additionally, brain masks or regional labels can be mapped from the group template to the SSTs so that volume change of any brain regions can be measured at the individual level.

2.3. Hierarchical voxel-wise detection of treatment effect

Voxel-wise detection of treatment effect was performed with the 3D Jacobian maps (as voxel-level measure of volume) across visits. Brain MRI data from OPERA I and OPERA II were analyzed independently using the Analysis of Functional NeuroImages (AFNI) software suite (Cox, 1996). Within each OPERA study, we employed a hierarchical analysis scheme that consisted of two steps. The first step consisted of simple linear regression of the voxel-wise Jacobian against time, regardless of treatment. This was iterated over all the voxels in the whole brain mask to identify brain regions with significant volume change during the entire trial period. For the second step, voxel-wise repeated two-way analysis of variance (ANOVA) of Treatment and Time was iterated over all the voxels in the regions of significant volume changes as identified at the first step. The second-step analysis was to identify a treatment effect of OCR on regional volume changes over time. This analysis was performed over the detected regions of significant shrinkage or significant expansion. At both steps of the hierarchical analysis, multiple test correction was applied across all the voxels in the whole brain mask based on family-wise error rate, which was performed with a cluster-based statistical method implemented in AFNI. Monte Carlo simulations with 10,000 iterations were done to determine how large a cluster of voxels was required to be statistically meaningful (Forman et al., 1995). Given the size of the whole brain mask, the minimum cluster extent was estimated at $7,966 \text{ mm}^3$ to reach $p < 0.05$ at both the voxel and cluster levels. The patient sample size was matched at $n = 285$ in each treatment arm of each OPERA study based on data availability at all visits after image processing and quality assessment, in both steps of the voxel-wise analysis. The sample matching at every visit was required by the voxel-wise repeated two-way ANOVA as implemented in AFNI, in order to have equal samples in each combination of factor levels.

2.4. Cross-study validation

The cross-study validation was performed to confirm that treatment effects were presented similarly in the two OPERA studies. For the brain region that was detected in one OPERA study, we evaluated whether the treatment effect was similarly presented in the same brain region in the other OPERA study. By extracting the mean Jacobian (as a measure of volume) of the detected region, we first performed repeated two-way ANOVA of Treatment and Time on the mean Jacobian of the detected brain region, which was a comparable analysis with the voxel-wise two-way ANOVA as described in the hierarchical analysis. In addition, we fit a linear mixed effects (LME) model for each detected region, which had the same primary formulation as the repeated two-way ANOVA to assess the interaction of Treatment and Time on the mean Jacobian, but adjusting for the following covariates: age, sex, geographical region of patient (USA versus the rest of the world), baseline measures of body mass index, whole brain volume, T1 gadolinium-enhancing lesion count, T2 lesion volume, unenhanced T1 lesion volume, as well as total change of unenhanced T1 lesion volume at Week 96 from baseline. All these covariates were obtained from the original analysis of the OPERA studies (Hauser et al., 2017b). The inclusion of both T2 lesion volume

and T1 gadolinium-enhancing lesion count at baseline was to take into account of possible influence of global neuroinflammation on regional brain volume changes. The inclusion of unenhanced T1 lesion volume, both at baseline and total change during the entire trial period, was mainly to control potential influence of white matter lesions on image registration between T1-weighted images in the longitudinal DBM pipeline, although the change of unenhanced T1 lesion volume was generally small over the 96-week trial period. Furthermore, the LME modelling was repeated after rebaselining to Week 24, in order to reduce the influence of potential pseudoatrophy in the first few months of the trials (Zivadinov et al., 2008). The analysis of the mean Jacobian was performed with the R software (version 3.5.2), in which the LME modelling was done with the lmerTest library (Kuznetsova et al., 2017). Outliers in each volumetric measure of the detected brain regions were defined as being outside the 99% confidence interval and, thus, were excluded from analysis.

2.5. Association with disability progression

We finally assessed the relationship of volume change in the detected brain region with disability progression with the pooled sample of OPERA I and OPERA II. This was performed on the overlap (intersection) mask of the detected regions from the two OPERA studies. Given the underlying different neuroanatomy and functions, different brain structures may have different relationships with disability progression. For this consideration, we identified individual anatomical structures that showed a substantial presence of detected voxels within the overlap mask, and then we assessed how volume change of each individual structure might be related to disability progression. The boundaries of individual brain structure were based on the Mindboggle brain atlas.

Confirmed disability progression (CDP) was defined as a composite measure of three clinical assessment methods: EDSS, Timed 25-Foot Walk (T25FW, a measure of short distance walking speed), and Nine-Hole Peg Test (9HPT, a measure of upper limb function) (Elliott et al., 2019). The 24-week CDP was defined as progression on any one of the three components (EDSS, T25FW, or 9HPT): an increase of EDSS score from the baseline by at least 1.0 point (or 0.5 points if the baseline EDSS score was > 5.5) or a 20% minimum threshold change for T25FW and 9HPT. This composite measure was able to capture a broader aspect of disability in patients with multiple sclerosis, which complemented the conventional EDSS score with meaningful measurements of body movement in both upper and lower limbs (Cadavid et al., 2017).

The main analysis of 24-week CDP was done in the comparator IFN β -1a arm, for the consideration that the highly effective OCR treatment might have a more direct relationship than brain volume measures with disease progression. For additional context, we also repeated the whole analysis of CDP in the OCR arm. Cox regression models were fit to assess the effect of percent volume change in the whole trial period on the time to the 24-week CDP based on the composite score, adjusting for age, sex, geographical region of patient (USA versus the rest of the world), study (OPERA I versus OPERA II), baseline measures of body mass index, whole brain volume, unenhanced T1 lesion volume, T1 gadolinium-enhancing lesion count, T2 lesion volume, total change of unenhanced T1 lesion volume at Week 96 from baseline, and baseline measures of three clinical measures which were included in the CDP assessment (EDSS, T25FW, and 9HPT). The rationale of adjusting for the lesion-based measures was the same as described in the cross-study validation. Furthermore, the Cox modelling was repeated after rebaselining the volume changes to Week 24.

3. Results

3.1. Hierarchical voxel-wise analysis and cross-study validation

At the first level of analysis of each OPERA study, significant volume change at the voxel-level were detected (Fig. S1). Proportions of

significant volume shrinkage or expansion was assessed in six major brain regions based on the Mindboggle atlas, including cerebrospinal fluid (CSF), cortical grey matter, deep grey matter, white matter, the brainstem, and the cerebellum (Table S2). The detected brain regions of significant volume change were similar between the two OPERA studies. As expected, significant volume shrinkage was found mainly in grey and white matter regions, while significant volume expansion was found mainly in CSF. It is also noted that a small portion of grey and white matter regions were identified as expansion, while a small portion of CSF regions were identified as shrinkage, which were likely caused by the partial volume effect in MRI for the limited image resolution.

3.1.1. Treatment effect in the regions of shrinkage

In OPERA I, a set of clustering voxels (48.1 cm^3) in the regions of shrinkage were detected with a significant treatment effect ($p < 0.05$, corrected at the cluster level). This encompassed parts of the thalamus, putamen, brainstem, neocortex (including insula, inferior frontal gyrus, precentral gyrus), in addition to some white matter near the corticospinal tract as well as in the cerebellum (Fig. 2A). By extracting the mean Jacobian of this detected region in OPERA I, the percent volume reduction from baseline was numerically less in the OCR arm at every follow-up visit, in comparison with the comparator IFN arm (Fig. 2B). Repeated two-way ANOVA confirmed a significant interaction between Treatment and Time on the mean Jacobian of the detected cluster ($F = 53.1, p < 0.001$), which indicated a treatment effect on time-related volume change. Adjusting for the specified covariates, the LME model confirmed a same treatment effect ($F = 53.0, p < 0.001$), which remained significant after rebaselining at Week 24 ($F = 18.6, p < 0.001$). Consistently, by extracting the mean Jacobian of the same brain region from the images of OPERA II, the percent volume reduction from

baseline was also numerically less in the OCR arm at every follow-up visit, in comparison with the comparator IFN arm (Fig. 2C). Repeated two-way ANOVA confirmed a significant interaction between Treatment and Time on the mean Jacobian ($F = 58.8, p < 0.001$), as well as the LME models either with the baseline ($F = 56.9, p < 0.001$) or after rebaselining at Week 24 ($F = 14.5, p < 0.001$).

For cross-study validation, the hierarchical voxel-wise analysis in the regions of shrinkage was repeated in OPERA II. A significant treatment effect was detected in similar brain regions of shrinkage as detected in OPERA I, in addition to parts of the posterior cingulate cortex, parietal and temporal cortices, and some white matter in corpus callosum (88.9 cm^3 , Fig. 2D). By extracting the mean Jacobian of this detected region in OPERA II, the percent volume reduction from baseline was numerically less in the OCR arm at each follow-up visit, in comparison with the comparator IFN arm (Fig. 2F). Repeated two-way ANOVA confirmed a significant interaction between Treatment and Time on the mean Jacobian ($F = 120.8, p < 0.001$), as well as the LME model either with the original baseline ($F = 117.9, p < 0.001$) or after rebaselining at Week 24 ($F = 44.0, p < 0.001$). Consistently, by extracting the mean Jacobian of the same brain region mask from the images of OPERA I, the percent volume reduction from baseline was numerically less in the OCR arm at each follow-up visit, in comparison with the comparator IFN arm (Fig. 2E). Repeated two-way ANOVA confirmed a significant interaction between Treatment and Time on the mean Jacobian ($F = 24.0, p < 0.001$), as well as the LME models either with the original baseline ($F = 23.3, p < 0.001$) or after rebaselining at Week 24 ($F = 11.0, p < 0.001$).

We extracted an overlap mask (13.30 cm^3) that was identified with a significant treatment effect in both OPERA I and OPERA II (Fig. 2G). The overlap mask contained 12.3% of the thalamus (1.9 cm^3), 27.1% of brainstem (4.8 cm^3), and 3.6% of cerebellum (5.1 cm^3 , mainly in white

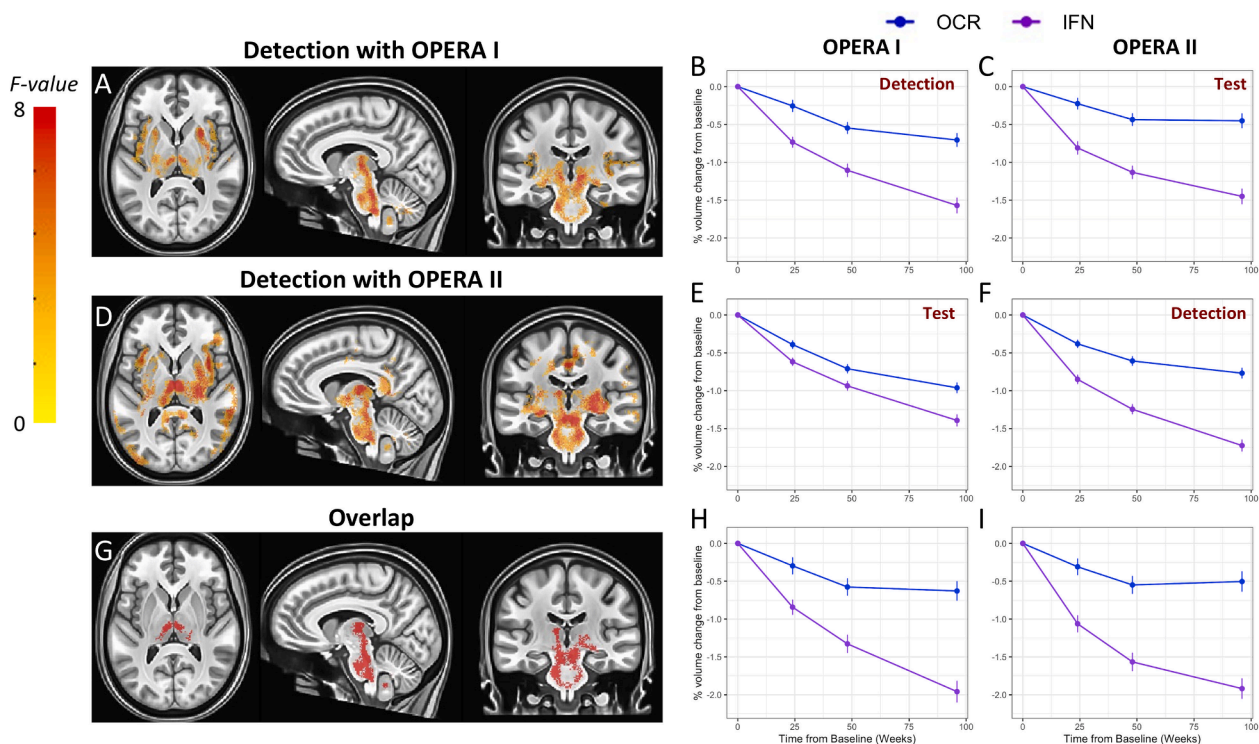


Fig. 2. Detection of treatment effects in the brain regions with significant volume shrinkage. (A) The F -value map of significant interaction between Treatment and Time on Jacobian (as a measure of volume) in the voxel-wise repeated two-way ANOVA, which indicates a significant treatment effect on volume change over time, in OPERA I. Percent volume change from baseline (based on mean Jacobian) of the detected region is plotted for (B) OPERA I and (C) OPERA II, for which OPERA II serves as an independent test set. (D) The F -value map of significant interaction between Treatment and Time on Jacobian in the voxel-wise repeated two-way ANOVA, in OPERA II. The percent volume change from baseline of the detected region is plotted for (E) OPERA I and (F) OPERA II, for which OPERA I serves as an independent test set. (G) Overlap of the detections in (A) and (D). The percent volume change from baseline in the overlap region is plotted for (H) OPERA I and (I) OPERA II. The colour bar indicates the magnitude of F -values in (A) and (D). The patient sample size was matched at $n = 285$ in each treatment arm of each OPERA study. Error bars indicate standard error.

matter). By extracting the mean Jacobian of this overlap mask, the percent volume reduction from baseline was numerically less in the OCR arm at each follow-up visit in both OPERA studies (Fig. 2H and I). The LME models confirmed a significant interaction between Treatment and Time on the mean Jacobian in both OPERA studies, either with the original baseline or after rebaselining at Week 24 ($F > 22.0$, $p < 0.001$).

3.1.2. Treatment effect in the regions of expansion

In OPERA I, a significant treatment effect in the regions of expansion was detected mainly in the lateral and third ventricles (32.3 cm³, Fig. 3A). By extracting the mean Jacobian of this detected region from the images in OPERA I, the percent volume increase from baseline was numerically less in the OCR arm at every follow-up visit, in comparison with the comparator IFN arm (Fig. 3B). Repeated two-way ANOVA confirmed a significant interaction between Treatment and Time on the mean Jacobian of the detected cluster ($F = 60.5$, $p < 0.001$), as well as the LME model with the original baseline ($F = 58.8$, $p < 0.001$) or after rebaselining at Week 24 ($F = 4.7$, $p = 0.03$). Consistently, by extracting the mean Jacobian of the same brain region from the images of OPERA II, the percent volume increase from baseline was numerically less in the OCR arm at every follow-up visit, in comparison with the comparator IFN arm (Fig. 3C). Repeated two-way ANOVA confirmed a significant interaction between Treatment and Time on the mean Jacobian ($F = 137.7$, $p < 0.001$), as well as the LME models either with the original baseline ($F = 130.7$, $p < 0.001$) or after rebaselining at Week 24 ($F = 41.0$, $p < 0.001$).

For cross-study validation, the hierarchical voxel-wise analysis in the regions of expansion was repeated in OPERA II. Two clusters of voxels were detected with a total volume of 65.0 cm³. One cluster contained the lateral and third ventricles, similar to what was detected in OPERA I.

The other cluster was located near the primary motor cortex (Fig. 3D). By extracting the mean Jacobian of the entire detected region from the images in OPERA II, the percent volume increase from baseline was numerically less in the OCR arm at every follow-up visit, in comparison with the comparator IFN arm (Fig. 3F). Repeated two-way ANOVA confirmed a significant interaction between Treatment and Time on the mean Jacobian ($F = 67.6$, $p < 0.001$), as well as the LME model either with the original baseline ($F = 61.6$, $p < 0.001$) or after rebaselining at Week 24 ($F = 15.9$, $p < 0.001$). Consistently, by extracting the mean Jacobian of the same brain region mask from the images of OPERA I, the percent volume increase from baseline was also numerically less in the OCR arm across follow-up visits, in comparison with the comparator IFN arm (Fig. 3E). Repeated two-way ANOVA confirmed a significant interaction between Treatment and Time on the mean Jacobian ($F = 27.4$, $p < 0.001$), as well as the LME model with the original baseline ($F = 25.9$, $p < 0.001$). This treatment effect, however, was not significant after rebaselining at Week 24 ($F = 1.5$, $p = 0.21$).

We extracted an overlap masks (29.1 cm³) of the brain regions of expansion that were identified with a significant treatment effect in both OPERA I and OPERA II (Fig. 3G). The overlap mask contained 85.4% of the lateral and third ventricles (13.3 cm³) in addition to some adjacent white matter. By extracting the mean Jacobian of the overlap mask, the treatment response was present in both OPERA studies (Fig. 3H and I). The LME models confirmed a significant treatment effect in both OPERA studies with the baseline ($F = 58.0$ in OPERA I; $F = 131.8$ in OPERA II; both $p < 0.001$), and a weaker but significant effect after rebaselining at Week 24 ($F = 4.8$, $p = 0.03$ in OPERA I; $F = 41.1$, $p < 0.001$ in OPERA II).

3.1.3. Identified subregions within individual brain structures

For further analysis of the relationship with disability progression,

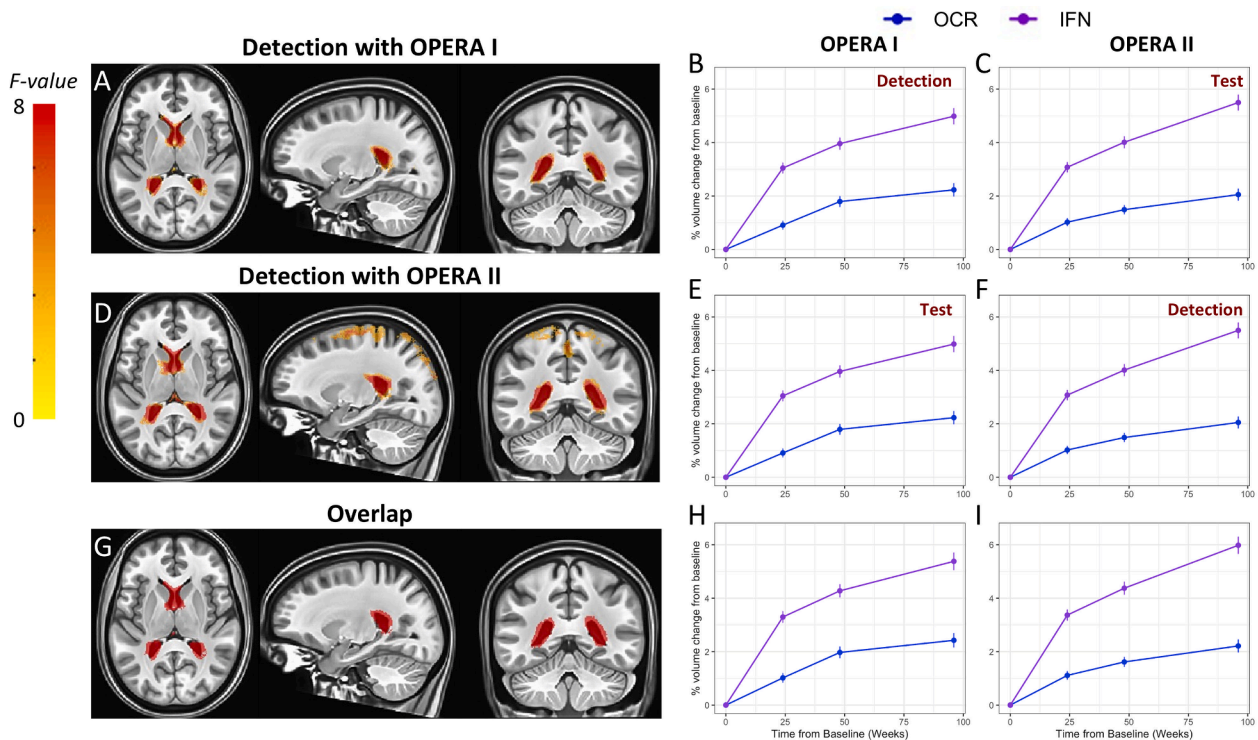


Fig. 3. Detection of treatment effects in the brain regions with significant volume expansion. (A) The F -value map of significant interaction between Treatment and Time on Jacobian (as a measure of volume) in the voxel-wise repeated two-way ANOVA, which indicates a significant treatment effect on volume change over time, in OPERA I. The percent volume change from baseline (based on mean Jacobian) of the detected region is plotted for (B) OPERA I and (C) OPERA II, for which OPERA II serves as an independent test set. (D) The F -value map of significant interaction between Treatment and Time on Jacobian in the voxel-wise repeated two-way ANOVA, in OPERA II. The percent volume change from baseline of the detected region is plotted for (E) OPERA I and (F) OPERA II, for which OPERA I serves as an independent test set. (G) Overlap of the detections in (A) and (D). The percent volume change from baseline in the overlap region is plotted for (H) OPERA I and (I) OPERA II. The colour bar indicates the magnitude of F -values in (A) and (D). The patient sample size was matched at $n = 285$ in each treatment arm of each OPERA study. Error bars indicate standard error.

four subregions of individual brain structures were identified with a significant treatment effect in both OPERA I and OPERA II (thalamus; brainstem; cerebellum in the regions of shrinkage; lateral and third ventricles in the regions of expansion; Fig. 4). With the pooled sample of OPERA I and OPERA II ($N = 1483$), the percent volume change from baseline in all the four subregions, regardless of shrinkage or expansion, was numerically less in the OCR arm at every follow-up visit, in comparison with the comparator IFN arm. The difference between the two treatment arms was the largest at the last visit (Week 96) when the percent volume change was estimated from the baseline (Cohen's $d = 0.58, 0.54, 0.33$ versus 0.67 , for the subregions of the thalamus, brainstem, cerebellum, lateral and third ventricles, respectively) or after rebaselining at Week 24 (Cohen's $d = 0.24, 0.37, 0.16$ versus 0.24 for the subregions of the thalamus, brainstem, cerebellum, lateral and third

ventricles, respectively). The LME models confirmed a significant interaction between Treatment and Time on the mean Jacobian of each of the four subregions either with the baseline ($F = 122.5, 122.2, 51.7$ versus 207.6 , for detected subregions of the thalamus, brainstem, cerebellum, lateral and third ventricles, respectively; $p < 0.001$ for all) or after rebaselining at Week 24 ($F = 28.7, 48.3, 11.6$ versus 46.9 , for detected subregions of the thalamus, brainstem, cerebellum, lateral and third ventricles, respectively; $p < 0.001$ for all).

For a reference, we performed a similar analysis with whole brain volume data rebaselining at Week 24, which were estimated by SIENA in the original clinical trial (Hauser et al., 2017b). Consistently, mean percent reduction of whole brain volume was less in the OCR arm than the comparator arm, and the difference between the two arms was larger at the last visit (Cohen's $d = 0.21$). In addition, the LME model

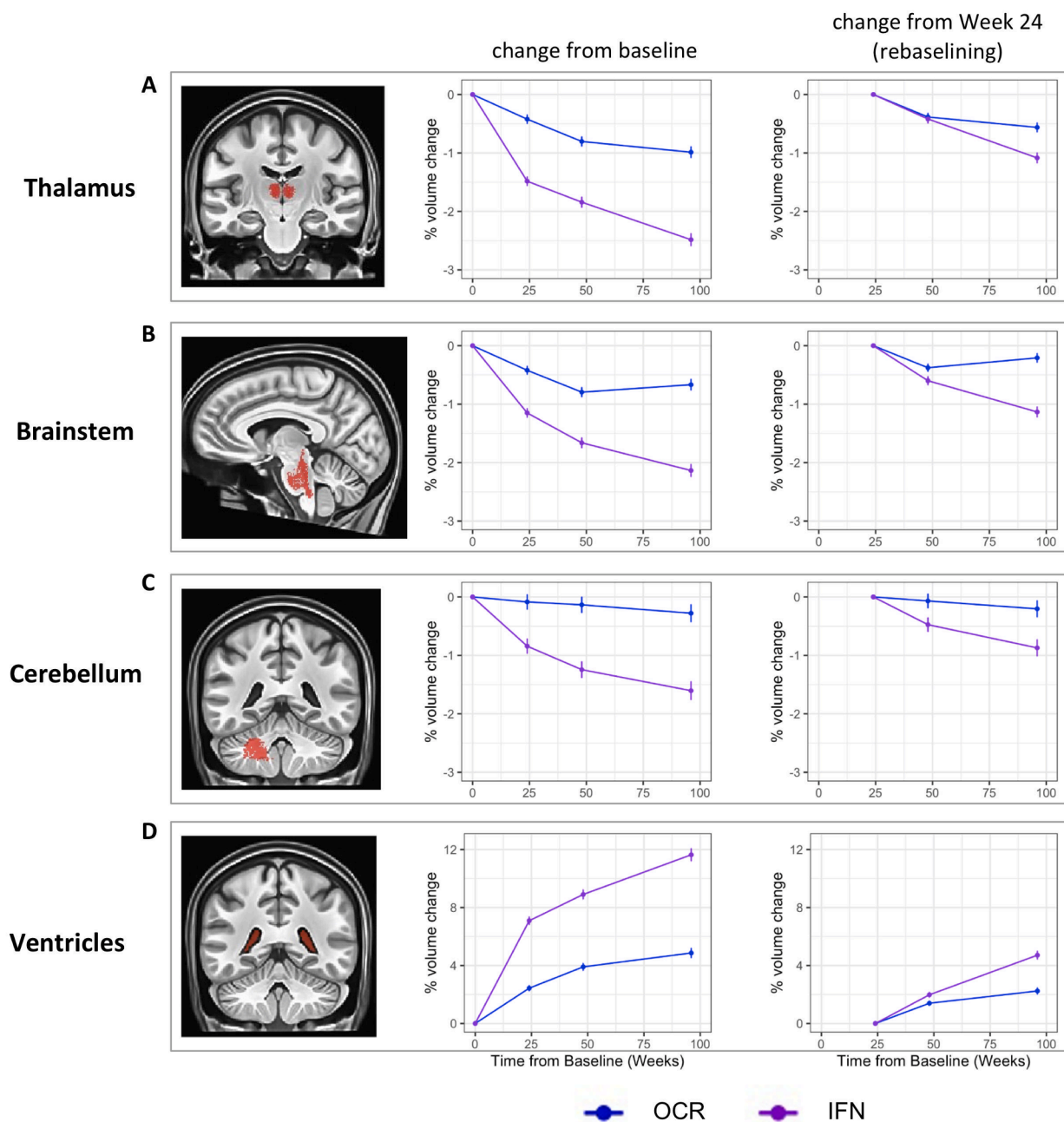


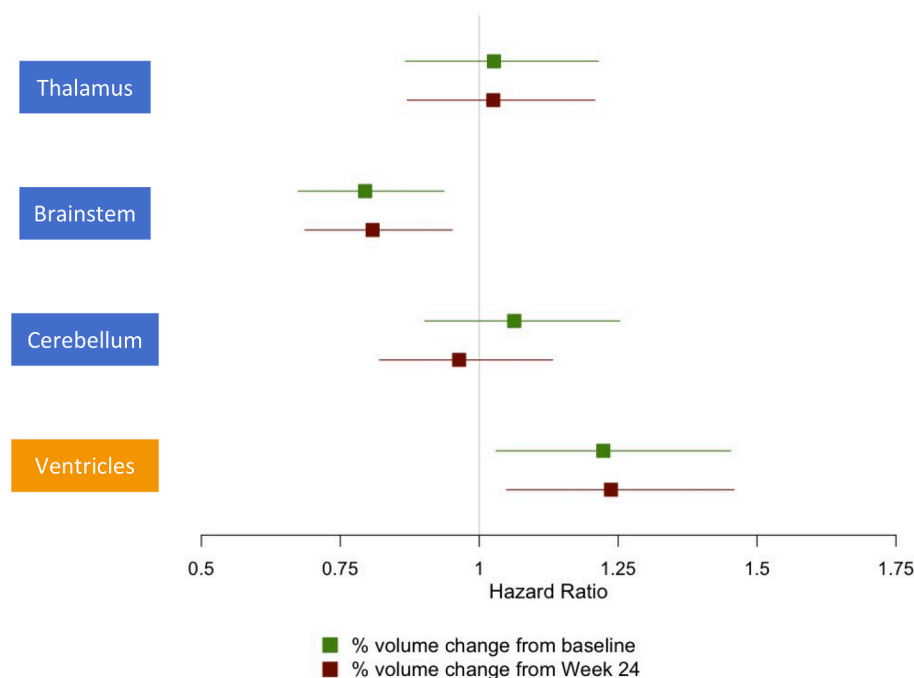
Fig. 4. Treatment effects in the identified subregions within individual brain structures. The masks of identified subregions are shown for (A) the thalamus, (B) brainstem, (C) cerebellum, and (D) lateral and third ventricles, each of which is followed by plots of the percent volume change from baseline and from Week 24 (after rebaselining), respectively, in each treatment arm, using the pooled sample of the two OPERA studies ($N = 1483$). Error bars indicate standard error.

confirmed a significant interaction between Treatment and Time ($F = 17.8, p < 0.001$). These results indicated a smaller treatment effect in the whole brain than the detected individual brain regions except the one in cerebellum.

3.2. Association with disability progression

In the comparator arm (treated with IFN β -1a) of OPERA I and OPERA II combined ($N = 596$), we fitted a series of Cox proportional hazards models to assess whether the percent volume change in each detected subregion in the brain was associated with time to the 24-week CDP. The percent volume change was estimated from either the baseline or Week 24 (rebaselining) to the end of the trial period (Week 96), and was normalized by z-scoring across patients for each brain region. Fig. 5 shows the estimated hazard ratio and 95% confidence interval of the percent volume change in the detected subregions. The percent volume reduction in the detected subregion of the brainstem was significantly associated with a higher risk of the 24-week CDP, with the volume change estimated from either the baseline ($p = 0.006$) or Week 24 ($p = 0.011$). This relationship was not significant in the detected subregion within either the thalamus or the cerebellum. In addition, the percent volume increase in the ventricles was significantly associated with a higher risk of the 24-week CDP, with the volume change estimated from either the baseline ($p = 0.021$) or Week 24 ($p = 0.012$). After multiple test correction of the false discovery rate across all of the above tests, the findings in both the brainstem and ventricles remained significant, with the volume change estimated from either the baseline or Week 24 ($p < 0.05$). As a reference, we performed a similar Cox modeling with the whole brain volume data as estimated by SIENA in the original trial report (Hauser et al., 2017b), and found that the total percent volume reduction of the whole brain volume at Week 96 from Week 24 (rebaselining) was not significantly associated with the 24-week CDP ($p = 0.15$).

For additional context, we repeated the Cox modeling in the OCR arm of OPERA I and OPERA II combined ($N = 655$), but there was no significant relationship between the 24-week CDP and the percent volume change of any detected subregions, with the volume change estimated either from the baseline or Week 24 ($p > 0.05$, uncorrected).



4. Discussion

This work focuses on the development and the application of a longitudinal DBM method to assess voxel-level brain volume changes in multiple sclerosis and its potential to advance imaging biomarker development with a focus on treatment response and disease progression. In our analysis of two independent pivotal trials of OCR in relapsing multiple sclerosis, a cluster of voxels of shrinkage were identified, including subregions within the thalamus and brainstem, where the percent volume loss was significantly reduced by the OCR treatment during the trial period, in comparison with the IFN β -1a response. The volume increase of brain ventricles, which reflected global brain atrophy, was also reduced by OCR. Importantly, the percent volume change in the brainstem and ventricles was significantly associated with a higher risk of the 24-week CDP in the comparative arm. Furthermore, the treatment effect was significant but less on the whole brain volume as assessed in the original OPERA trials (Hauser et al., 2017b). In addition, change of the whole brain volume was not significantly correlated with disability progression. All these findings together support the view that localized brain volume change can be more sensitive to effective therapeutic interventions as well as being more correlated with disease progression, and that these local changes may be muted when atrophy estimates are made over the whole brain.

The DBM analysis of brain volume changes relied on precise nonlinear image registration across time points of each patient in the longitudinal pipeline. In contrast to voxel-based morphometry, which has been applied to multiple sclerosis research albeit with only limited success (Sastre-Garriga et al., 2020), DBM doesn't require tissue segmentation. Hence its performance is immune to segmentation errors. Given its validated performance of brain image registration (Avants et al., 2011; Klein et al., 2009), the ANTs method has been applied to multiple sclerosis research, mainly by atlas-based Jacobian integration (Andorra et al., 2018; Fadda et al., 2019; Nakamura et al., 2014). The present longitudinal DBM pipeline further minimizes registration errors by constructing and utilizing an unbiased SST as the reference image for the patient level analysis, where the SST had minimum anatomical difference with individual images of the same patient.

The underlying mechanism of brain atrophy in multiple sclerosis remains to be elucidated (Calabrese et al., 2015). Since brain atrophy is

Fig. 5. Association of the percent volume changes in the identified subregions within individual brain structures with disability progression. The identified subregions were within the thalamus, brainstem, cerebellum, and lateral and third ventricles, respectively. Cox regression models were fit to assess the effect of percent volume change in each identified structure on the 24-week CDP, in the comparator arm (treated with IFN β -1a) of the two OPERA studies together ($n = 596$). Forest plots of hazard ratio and 95% confidence interval are provided for the identified structures. The percent volume change was assessed from either baseline (green) or Week 24 (rebaselining, red), and was normalized by z-scoring for each region. Blue boxes indicate shrinkage and orange indicates expansion. The number of patients who had an event of the 24-week CDP was 174 in this sample. (For interpretation of the references to colour in this figure legend, the reader is referred to the web version of this article.)

a part of normal aging and many other neurological diseases (Azevedo et al., 2019), it is not straightforward to identify multiple sclerosis-specific atrophy with conventional brain MRI. Some evidence suggests that inflammation-induced axonal transection in the connecting fibre tracts may be a major cause of neuronal loss in multiple sclerosis (Cifelli et al., 2002). In addition, *trans*-synaptic degeneration may also play an important role (Ontaneda et al., 2021), which allows neuronal injury to spread from neuron to neuron through synaptic connection in the brain network and thus offers an insight about the spatial distribution of brain atrophy.

As an increase of ventricular volume reflects global brain atrophy, a suppression of ventricular volume increase by OCR treatment indicates a global improvement against brain atrophy. Given the likely non-random spatial distribution of brain atrophy (Steenwijk et al., 2016) and variable treatment response across brain structures, a suppression of volume loss in specific brain regions may reflect the treatment effect at a finer scale. Among the identified brain structures, involvement of the thalamus in multiple sclerosis has attracted significant attention in recent years (Amin and Ontaneda, 2020; Fadda et al., 2019; Zivadinov et al., 2013). The thalamus has extensive neural connections with major cortical and subcortical structures, which makes it relevant to a wide range of brain functions including sensory, motor, and cognitive functions. For the same reason, the thalamus may be particularly sensitive to both diffusive neurodegeneration via the mechanism of *trans*-synaptic degeneration, as well as being responsive to neuroprotective therapies (Kipp et al., 2015). However, the involvement of thalamus in movement-related functions is not fully understood (Sommer, 2003). Although baseline thalamic volume has been related to clinical progression of patients with relapsing multiple sclerosis in a few studies (Eshaghi et al., 2018b), to the best of our knowledge, an association between thalamic volume change and CDP has not yet been reported. Our data showed no significant association of the percent volume change with the risk of the 24-week CDP, in the detected subregion of the thalamus. A plausible reason might be that the composite disability score used in our analysis did not capture the thalamic role in the measured disabilities of this patient population.

Relatively few neuroimaging studies in multiple sclerosis have been dedicated to the brainstem or cerebellum, although both structures are highly relevant to the pathology and clinical characteristics of multiple sclerosis (Comi et al., 1993; Habek, 2013; Magnano et al., 2014; Nakashima et al., 1999). Our finding in the brainstem was particularly interesting for the significant association between its volume loss and the risk of the 24-week CDP. This association is aligned with the strong neural connectivity of the brainstem with both the spinal cord and motor cortex via the corticospinal tract (Kerbrat et al., 2020). Spinal cord lesions are strongly associated with movement-related disability in multiple sclerosis (Sastre-Garriga et al., 2020; Schlaeger et al., 2015; Tsagkas et al., 2019). Spinal damage could potentially manifest in the brainstem due to *trans*-synaptic degeneration (Ontaneda et al., 2021). Spine MRI is often technically much more difficult than brain MRI (Sastre-Garriga et al., 2020). There are some recent efforts to measure atrophy of upper cervical cord with brain MRI (Lundell et al., 2017). Nonetheless, the ability to assess the brainstem atrophy in brain MRI may be potentially a useful surrogate biomarker of spinal atrophy.

The cerebellum is another important brain structure whose involvement in multiple sclerosis has been increasingly recognized (Parmar et al., 2018). Our detection of the treatment effect of OCR in the cerebellum, however, was rather small (3.6% of the whole cerebellum), which was mainly located in white matter. This limited finding might be due to contamination by the CSF signal in the tightly folded cortical grey matter (the folia) of the cerebellum. Due to the small detection size, the pattern of volume change in the detected part might not be representative of the whole cerebellum, when the grey matter compartment was largely excluded from the first-level analysis of volume change regardless of treatment.

One limitation of the present study was due to the partial volume effect in the original brain MRI of the OPERA trials, given the slice

thickness of 3 mm, while the in-plane resolution was good at $1 \times 1 \text{ mm}^2$. Brain tissues and CSF regions may undergo opposite volume changes in the process of neurodegeneration. Specifically, when there is volume loss in grey or white matter, it is often accompanied with a volume increase in adjacent CSF. To reduce the impact of this problem, we adopted a hierarchical analysis scheme, in which the detection of treatment effect was restricted to brain regions that demonstrated either significant volume loss or significant volume increase. Nonetheless, the voxel-level analysis can be more reliable with use of higher resolution brain MRI sequences, especially in the highly folded cerebral and cerebellar cortices. This explains that our major findings were in deep grey matter regions, where the MRI signal was less affected by partial volume effects given the anatomy.

Another technical challenge of brain atrophy assessment was due to the presence of visible lesions in multiple sclerosis (Sastre-Garriga et al., 2020). In contrast to segmentation-based volume estimation methods (e.g., FreeSurfer), the impact of lesions on the DBM analysis is more indirect by compromising the quality of voxel-wise image registration, which assumes a voxel-wise correspondence between each individual brain image and the reference image (either the SST or the group template). This assumption is violated if there are substantially different lesion profiles between images. For the longitudinal DBM, the impact of lesions would be greater if there are larger changes in lesion profiles over time within each patient because the main assessment is done at the patient-level. This is often less the case for lesions that are visible in unenhanced T1-weighted MRI, which are generally chronic lesions and tend to be smaller and the change is slower, comparing to lesions visible in T2-weighted MRI or contrast enhanced T1 lesions that indicate active neuroinflammation. Although it is a common practice to do artificial lesion filling in order to minimize the impact of lesions in brain atrophy assessments (Sastre-Garriga et al., 2020), a major concern is that lesion masks are often imprecise. Inter-rater agreement of lesion segmentation in multiple sclerosis is overall <70% among trained radiologists, and this number is even lower for smaller lesions (Egger et al., 2017). In addition, intensity sampling used for lesion filling is not trivial given the heterogeneity of image intensity in brain MRI, even within a same tissue type. To address the potential need for lesion filling, we ran a test with the OPERA I data set using a commonly used lesion filling method in FSL (Battaglini et al., 2012) but did not find it beneficial in our analysis of treatment effects (Fig. S2). For the above reasons, we elected not to do lesion filling for the present study. Nonetheless, future decisions may be conditional to the nature of specific data and subject to the availability of methodological advances in nonlinear image registration which minimize the effects of lesions.

A further complication of interpretation was due to the complex nature of brain volume changes with anti-inflammatory treatments. It has been long thought that short-term changes in the brain (e.g., water loss) during the treatment with anti-inflammatory DMTs in multiple sclerosis may cause additional brain volume changes, which is often termed as pseudoatrophy because it is not associated with real cell loss (Sastre-Garriga et al., 2020; Zivadinov et al. 2008, 2016). Some studies suggest that pseudoatrophy may be mainly confined to white matter (Vidal-Jordana et al., 2013). Nonetheless, it remains unclear how to distinguish pseudoatrophy from true atrophy (De Stefano and Arnold, 2015; Sastre-Garriga et al., 2020; Zivadinov et al., 2016). The interpretation of our data may be further complicated by the lack of placebo group in the OPERA trials because pseudoatrophy might occur not only in the OCR arm but also in the comparator arm that was treated with IFN, especially in the first few months (Dwyer et al., 2015). A commonly accepted guideline, although not completely certain, is to perform a rebaselining measurement of brain volume change at 6–12 months after initiation of any anti-inflammatory treatments (Sastre-Garriga et al., 2020). This may not be an optimal solution because some important treatment effect may have already occurred in the first several months (Zivadinov et al., 2016). Given this complexity, we took a complementary approach in the present work. We first conducted voxel-wise

analysis with all the time points, including the baseline visit. Then we analyzed the mean Jacobian data (a measure of volume) of the identified regions with and without rebaselining, respectively, in order to understand the differences between these two approaches. Although volume change was reduced after rebaselining to Week 24, the main findings of treatment effects remained significant after rebaselining.

In summary, the present work demonstrates that a data-driven longitudinal DBM method can generate valuable insights on how a DMT may modify localized brain atrophy, which may be missed by analyses with predefined brain regions. The findings of a therapeutic response in multiple brain structures likely reflects a widespread slowdown of brain atrophy as a positive response to treatment. Importantly, the percent volume loss in the brainstem, as well as the percent volume increase in the ventricles, was significantly associated with higher risk of disability progression. The present work has a strong implication for developing image-based biomarkers to advance future drug development for multiple sclerosis, where there is an increasing focus on the progressive biology.

5. Data availability

The fully anonymized, individual patient raw data including clinical and MRI data of the OPERA trials are made available through the International Progressive MS Alliance (www.progressivemsalliance.org).

Funding

All funding was internal to Genentech/Roche. No external funding was used for this work. Articulate Science, UK provided editorial finalization and was funded by F. Hoffmann-La Roche Ltd.

CRediT authorship contribution statement

Zhuang Song: Conceptualization, Data curation, Formal analysis, Validation, Visualization, Investigation, Methodology, Software, Writing – original draft, Writing – review & editing. **Anithapriya Krishnan:** Conceptualization, Investigation, Methodology, Writing – review & editing. **Laura Gaetano:** Conceptualization, Methodology, Writing – review & editing. **Nicholas J. Tustison:** Methodology, Software, Writing – review & editing. **David Clayton:** Conceptualization, Data curation, Resources, Writing – review & editing. **Alex de Crespiigny:** Conceptualization, Resources, Writing – review & editing. **Thomas Bengtsson:** Conceptualization, Supervision, Resources, Writing – review & editing. **Xiaoming Jia:** Conceptualization, Writing – review & editing. **Richard A.D. Carano:** Conceptualization, Methodology, Writing – original draft, Writing – review & editing, Supervision, Resources.

Declaration of Competing Interest

All authors except one (N.J.T.) are employees of Genentech/Roche and are stockholders of Roche.

Acknowledgements

We would like to thank Dr Denise Park at University of Texas at Dallas for making brain MRI data of healthy adults publicly available from the Dallas Lifespan Brain Study, Dr Jinglan Pei at Genentech for help on clinical data in the OPERA studies, and Dr Xiao Li at Genentech for insightful discussions on statistical methods.

Appendix A. Supplementary data

Supplementary data to this article can be found online at <https://doi.org/10.1016/j.nicl.2022.102959>.

References

- Amin, M., Ontaneda, D., 2020. Thalamic injury and cognition in multiple sclerosis. *Front. Neurol.* 11, 623914. <https://doi.org/10.3389/fneur.2020.623914>.
- Andorra, M., Nakamura, K., Lampert, E.J., Pulido-Valdeolivas, I., Zubizarreta, I., Llufríu, S., Martínez-Heras, E., Sola-Valls, N., Sepulveda, M., Tercero-Urbe, A., Blanco, Y., Saiz, A., Villoslada, P., Martínez-Lapiscina, E.H., 2018. Assessing biological and methodological aspects of brain volume loss in multiple sclerosis. *JAMA Neurol.* 75 (10), 1246–1255. <https://doi.org/10.1001/jamaneurol.2018.1596>.
- Ashburner, J., Friston, K.J., 2000. Voxel-based morphometry—the methods. *Neuroimage* 11 (6 Pt 1), 805–821. pii/S1053811900905822.
- Avants, B.B., Tustison, N.J., Song, G., Cook, P.A., Klein, A., Gee, J.C., 2011. A reproducible evaluation of ANTs similarity metric performance in brain image registration. *Neuroimage* 54 (3), 2033–2044. <https://doi.org/10.1016/j.neuroimage.2010.09.025>.
- Avants, B.B., Tustison, N.J., Stauffer, M., Song, G., Wu, B., Gee, J.C., 2014. The Insight ToolKit image registration framework. *Front. Neuroinform.* 8, 44. <https://doi.org/10.3389/fninf.2014.00044>.
- Avants, B.B., Yushkevich, P., Pluta, J., Minkoff, D., Korczynowski, M., Detre, J., Gee, J.C., 2010. The optimal template effect in hippocampus studies of diseased populations. *Neuroimage* 49 (3), 2457–2466.
- Azevedo, C.J., Cen, S.Y., Jaberzadeh, A., Zheng, L., Hauser, S.L., Pelletier, D., 2019. Contribution of normal aging to brain atrophy in MS. *Neurol. Neuroimmunol. Neuroinflamm.* 6 (6), e616. <https://doi.org/10.1212/NXL.0000000000000616>.
- Azevedo, C.J., Cen, S.Y., Khadka, S., Liu, S., Kornak, J., Shi, Y., Zheng, L., Hauser, S.L., Pelletier, D., 2018. Thalamic atrophy in multiple sclerosis: A magnetic resonance imaging marker of neurodegeneration throughout disease. *Ann. Neurol.* 83 (2), 223–234. <https://doi.org/10.1002/ana.25150>.
- Battaglini, M., Jenkinson, M., De Stefano, N., 2012. Evaluating and reducing the impact of white matter lesions on brain volume measurements. *Hum. Brain. Mapp.* 33 (9), 2062–2071. <https://doi.org/10.1002/hbm.21344>.
- Bullmore, E., Sporns, O., 2009. Complex brain networks: Graph theoretical analysis of structural and functional systems. *Nat. Rev. Neurosci.* 10 (3), 186–198. <https://doi.org/10.1038/nrn2575>.
- Cadavid, D., Cohen, J.A., Freedman, M.S., Goldman, M.D., Hartung, H.P., Havrdova, E., Jeffrey, D., Kapoor, R., Miller, A., Sellebjerg, F., Kinch, D., Lee, S., Shang, S., Mikol, D., 2017. The EDSS-Plus, an improved endpoint for disability progression in secondary progressive multiple sclerosis. *Mult. Scler.* 23 (1), 94–105. <https://doi.org/10.1177/1352458516638941>.
- Calabrese, M., Atzori, M., Bernardi, V., Morro, A., Romualdi, C., Rinaldi, L., McAuliffe, M.J.M., Barachino, L., Perini, P., Fischl, B., Battistin, L., Gallo, P., 2007. Cortical atrophy is relevant in multiple sclerosis at clinical onset. *J. Neurol.* 254 (9), 1212–1220. <https://doi.org/10.1007/s00415-006-0503-6>.
- Calabrese, M., Magliozzi, R., Ciccarelli, O., Geurts, J.J., Reynolds, R., Martin, R., 2015. Exploring the origins of grey matter damage in multiple sclerosis. *Nat. Rev. Neurosci.* 16 (3), 147–158. <https://doi.org/10.1038/nrn3900>.
- Chung, M.K., Worsley, K.J., Paus, T., Cherif, C., Collins, D.L., Giedd, J.N., Rapoport, J.L., Evans, A.C., 2001. A unified statistical approach to deformation-based morphometry. *Neuroimage* 14 (3), 595–606.
- Cifelli, A., Arridge, M., Jezzard, P., Esiri, M.M., Palace, J., Matthews, P.M., 2002. Thalamic neurodegeneration in multiple sclerosis. *Ann. Neurol.* 52 (5), 650–653. <https://doi.org/10.1002/ana.10326>.
- Comi, G., Filippi, M., Martinelli, V., Scotti, G., Locatelli, T., Medaglini, S., Triulzi, F., Rovaris, M., Canal, N., 1993. Brain stem magnetic resonance imaging and evoked potential studies of symptomatic multiple sclerosis patients. *Eur. Neurol.* 33 (3), 232–237. <https://doi.org/10.1159/000116943>.
- Compston, A., Coles, A., 2008. Multiple sclerosis. *Lancet* 372 (9648), 1502–1517. [https://doi.org/10.1016/S0140-6736\(08\)61620-7](https://doi.org/10.1016/S0140-6736(08)61620-7).
- Cox, R., 1996. AFNI: software for analysis and visualization of functional magnetic resonance neuroimages. *Comput Biomed Res.* 29 (3), 162–173. <https://doi.org/10.1006/cbmr.1996.0014>.
- Cree, B.A.C., Hollenbach, J.A., Bove, R., Kirkish, G., Sacco, S., Caverzasi, E., Bischof, A., Gundel, T., Zhu, A.H., Papinutto, N., Stern, W.A., Bevan, C., Romeo, A., Goodin, D.S., Gelfand, J.M., Graves, J., Green, A.J., Wilson, M.R., Zamvil, S.S., Zhao, C., Gomez, R., Ragan, N.R., Rush, G.Q., Barba, P., Santaniello, A., Baranzini, S.E., Oksenberg, J.R., Henry, R.G., Hauser, S.L., 2019. Silent progression in disease activity-free relapsing multiple sclerosis. *Ann. Neurol.* 85 (5), 653–666. <https://doi.org/10.1002/ana.25463>.
- Dalton, C.M., Chard, D.T., Davies, G.R., Miszkil, K.A., Altmann, D.R., Fernando, K., Plant, G.T., Thompson, A.J., Miller, D.H., 2004. Early development of multiple sclerosis is associated with progressive grey matter atrophy in patients presenting with clinically isolated syndromes. *Brain* 127 (Pt 5), 1101–1107. <https://doi.org/10.1093/brain/awh126>.
- Desikan, R.S., Segonne, F., Fischl, B., Quinn, B.T., Dickerson, B.C., Blacker, D., Buckner, R.L., Dale, A.M., Maguire, R.P., Hyman, B.T., Albert, M.S., Killiany, R.J., 2006. An automated labeling system for subdividing the human cerebral cortex on MRI scans into gyral based regions of interest. *Neuroimage* 31 (3), 968–980. <https://doi.org/10.1016/j.neuroimage.2006.01.021>.
- De Stefano, N., Arnold, D.L., 2015. Towards a better understanding of pseudoatrophy in the brain of multiple sclerosis patients. *Mult. Scler.* 21 (6), 675–676. <https://doi.org/10.1177/1352458514564494>.
- De Stefano, N., Matthews, P.M., Filippi, M., Agosta, F., De Luca, M., Bartolozzi, M.L., Guidi, L., Ghezzi, A., Montanari, E., Cifelli, A., Federico, A., Smith, S.M., 2003. Evidence of early cortical atrophy in MS: Relevance to white matter changes and

- disability. *Neurology* 60 (7), 1157–1162. <https://doi.org/10.1212/01.wnl.0000055926.69643.03>.
- Dwyer, M.G., Zivadinov, R., Tao, Y., Zhang, X., Kennedy, C., Bergsland, N., Ramasamy, D.P., Duffe, J., Hojnacki, D., Weinstock-Guttman, B., Hayward, B., Dangond, F., Markovic-Plese, S., 2015. Immunological and short-term brain volume changes in relapsing forms of multiple sclerosis treated with interferon beta-1a subcutaneously three times weekly: An open-label two-arm trial. *BMC Neurol.* 15, 232. <https://doi.org/10.1186/s12883-015-0488-9>.
- Egger, C., Opfer, R., Wang, C., Kepp, T., Sormani, M.P., Spies, L., Barnett, M., Schippling, S., 2017. MRI FLAIR lesion segmentation in multiple sclerosis: Does automated segmentation hold up with manual annotation? *Neuroimage Clin.* 13, 264–270. <https://doi.org/10.1016/j.neuroimage.2017.03.028>.
- Elliott, C., Belachew, S., Wolinsky, J.S., Hauser, S.L., Kappos, L., Barkhof, F., Bernasconi, C., Fecker, J., Model, F., Wei, W., Arnold, D.L., 2019. Chronic white matter lesion activity predicts clinical progression in primary progressive multiple sclerosis. *Brain* 142 (9), 2787–2799. <https://doi.org/10.1093/brain/awz212>.
- Eshaghi, A., Marinescu, R.V., Young, A.L., Firth, N.C., Prados, F., Cardoso, M.J., Tur, C., De Angelis, F., Cawley, N., Brownlee, W.J., De Stefano, N., Stromillo, M.L., Battaglini, M., Ruggieri, S., Gasperini, C., Filippi, M., Rocca, M.A., Rovira, A., Sastre-Garriga, J., Geurts, J.J.G., Vrenken, H., Wottschel, V., Leurs, C.E., Uitdehaag, B., Pirpamer, L., Enzinger, C., Ourselin, S., Gandini Wheeler-Kingshott, C.A.M., Chard, D., Thompson, A.J., Barkhof, F., Alexander, D.C., Ciccarelli, O., 2018a. Progression of regional grey matter atrophy in multiple sclerosis. *Brain* 141 (6), 1665–1677. <https://doi.org/10.1093/brain/awy088>.
- Eshaghi, A., Prados, F., Brownlee, W.J., Altmann, D.R., Tur, C., Cardoso, M.J., De Angelis, F., van de Pavert, S.H., Cawley, N., De Stefano, N., Stromillo, M.L., Battaglini, M., Ruggieri, S., Gasperini, C., Filippi, M., Rocca, M.A., Rovira, A., Sastre-Garriga, J., Vrenken, H., Leurs, C.E., Killestein, J., Pirpamer, L., Enzinger, C., Ourselin, S., Gandini Wheeler-Kingshott, C.A.M., Chard, D., Thompson, A.J., Alexander, D.C., Barkhof, F., Ciccarelli, O., 2018b. MAGNIMS study group. Deep gray matter volume loss drives disability worsening in multiple sclerosis. *Ann. Neurol.* 83 (2), 210–222. <https://doi.org/10.1002/ana.25145>.
- Fadda, G., Brown, R.A., Magliozzi, R., Aubert-Broche, B., O'Mahony, J., Shinohara, R.T., Banwell, B., Marrie, R.A., Yeh, E.A., Collins, D.L., Arnold, D.L., Bar-Or, A., Network, C.P.D.D., 2019. A surface-in gradient of thalamic damage evolves in pediatric multiple sclerosis. *Ann. Neurol.* 85 (3), 340–351. <https://doi.org/10.1002/ana.25429>.
- Fischl, B., van der Kouwe, A., Destrieux, C., Halgren, E., Segonne, F., Salat, D.H., Busa, E., Seidman, L.J., Goldstein, J., Kennedy, D., Caviness, V., Makris, N., Rosen, B., Dale, A.M., 2004. Automatically parcellating the human cerebral cortex. *Cereb. Cortex* 14 (1), 11–22.
- Fisniku, L.K., Chard, D.T., Jackson, J.S., Anderson, V.M., Altmann, D.R., Miszkiel, K.A., Thompson, A.J., Miller, D.A., 2008. Gray matter atrophy is related to long-term disability in multiple sclerosis. *Ann. Neurol.* 64 (3), 247–254. <https://doi.org/10.1002/ana.21423>.
- Forman, S.D., Cohen, J.D., Fitzgerald, M., Eddy, W.F., Mintun, M.A., Noll, D.C., 1995. Improved assessment of significant activation in functional magnetic resonance imaging (fMRI): Use of a cluster-size threshold. *Magn. Reson. Med.* 33 (5), 636–647. <https://doi.org/10.1002/mrm.1910330508>.
- Habek, M., 2013. Evaluation of brainstem involvement in multiple sclerosis. *Expert. Rev. Neurother.* 13 (3), 299–311. <https://doi.org/10.1586/ern.13.18>.
- Haider, L., Zrzavy, T., Hametner, S., Höftberger, R., Bagnato, F., Grabner, G., Trattng, S., Pfeifering, S., Brück, W., Lassmann, H., 2016. The topography of demyelination and neurodegeneration in the multiple sclerosis brain. *Brain* 139 (Pt 3), 807–815. <https://doi.org/10.1093/brain/awv398>.
- Hauser, S.L., Bar-Or, A., Comi, G., Giovannoni, G., Hartung, H.P., Hemmer, B., Lublin, F., Montalban, X., Rammohan, K.W., Selman, K., Trabulsee, A., Wolinsky, J.S., Arnold, D.L., Klingenschmitt, G., Masterman, D., Fontoura, P., Belachew, S., Chin, P., Mairon, N., Garren, H., Kappos, L., 2017a. OPERA I and OPERA II Clinical Investigators. Ocrelizumab versus interferon beta-1a in relapsing multiple sclerosis. *N. Engl. J. Med.* 376 (3), 221–234. <https://doi.org/10.1056/NEJMoa1601277>.
- Hauser, S.L., Belachew, S., Kappos, L., 2017b. Ocrelizumab in primary progressive and relapsing multiple sclerosis. *N. Engl. J. Med.* 376 (17), 1694. <https://doi.org/10.1056/NEJMc1702076>.
- Hauser, S.L., Kappos, L., Arnold, D.L., Bar-Or, A., Brochet, B., Naismith, R.T., Trabulsee, A., Wolinsky, J.S., Belachew, S., Koendgen, H., Levesque, V., Manfrini, M., Model, F., Hubeaux, S., Mehta, L., Montalban, X., 2020. Five years of ocrelizumab in relapsing multiple sclerosis: OPERA studies open-label extension. *Neurology* 95 (13), e1854–e1867. <https://doi.org/10.1212/WNL.00000000000010376>.
- Kerbrat, A., Gros, C., Badji, A., Bannier, E., Galassi, F., Combès, B., Chouteau, R., Labauge, P., Aygnac, X., Carra-Dalliere, C., Maranzano, J., Granberg, T., Ouellette, R., Stawiarz, L., Hillert, J., Talbot, J., Tachibana, Y., Hori, M., Kamiya, K., Chougar, L., Lefevre, J., Reich, D.S., Nair, G., Valsasina, P., Rocca, M.A., Filippi, M., Chu, R., Bakshi, R., Callot, V., Pelletier, J., Audoin, B., Maarouf, A., Collongues, N., De Seze, J., Edan, G., Cohen-Adad, J., 2020. Multiple sclerosis lesions in motor tracts from brain to cervical cord: Spatial distribution and correlation with disability. *Brain* 143 (7), 2089–2105. <https://doi.org/10.1093/brain/awaa162>.
- Kipp, M., Wagenknecht, N., Beyer, C., Samer, S., Wuerfel, J., Nikoubashman, O., 2015. Thalamus pathology in multiple sclerosis: From biology to clinical application. *Cell. Mol. Life. Sci.* 72 (6), 1127–1147.
- Klein, A., Andersson, J., Ardekani, B.A., Ashburner, J., Avants, B., Chiang, M.C., Christensen, G.E., Collins, D.L., Gee, J., Hellier, P., Song, J.H., Jenkinson, M., Lepage, C., Rueckert, D., Thompson, P., Vercauteren, T., Woods, R.P., Mann, J.J., Parsey, R.V., 2009. Evaluation of 14 nonlinear deformation algorithms applied to human brain MRI registration. *Neuroimage* 46 (3), 786–802. <https://doi.org/10.1016/j.neuroimage.2008.12.037>.
- Klein, A., Tourville, J., 2012. 101 labeled brain images and a consistent human cortical labeling protocol. *Front. Neurosci.* 6, 171. <https://doi.org/10.3389/fnins.2012.00171>.
- Kuznetsova, A., Brockhoff, P.B., Christensen, R.H.B., 2017. lmerTest Package: Tests in Linear Mixed Effects Models. *J. Stat. Softw.* 82 (13), 1–26. <https://doi.org/10.18637/jss.v082.i13>.
- Lansley, J., Mataix-Cols, D., Grau, M., Radua, J., Sastre-Garriga, J., 2013. Localized grey matter atrophy in multiple sclerosis: A meta-analysis of voxel-based morphometry studies and associations with functional disability. *Neurosci. Biobehav. Rev.* 37 (5), 819–830. <https://doi.org/10.1016/j.neubiorev.2013.03.006>.
- Lundell, H., Svlogaard, O., Dogonowski, A.M., Romme Christensen, J., Selleberg, F., Soelberg Sorensen, P., Blinkenberg, M., Siebner, H.R., Garde, E., 2017. Spinal cord atrophy in anterior-posterior direction reflects impairment in multiple sclerosis. *Acta Neurol. Scand.* 136 (4), 330–337. <https://doi.org/10.1111/ane.12729>.
- Magnano, I., Pes, G.M., Pilurzi, G., Cabboi, M.P., Ginatempo, F., Giaconi, E., Tolu, E., Achene, A., Salis, A., Rothwell, J.C., Conti, M., Deriu, F., 2014. Exploring brainstem function in multiple sclerosis by combining brainstem reflexes, evoked potentials, clinical and MRI investigations. *Clin. Neurophysiol.* 125 (11), 2286–2296. <https://doi.org/10.1016/j.clinph.2014.03.016>.
- Manera, A.L., Dadar, M., Collins, D.L., Ducharme, S., Frontotemporal Lobar Degeneration Neuroimaging, I., 2019. Deformation-based morphometry study of longitudinal MRI changes in behavioral variant frontotemporal dementia. *Neuroimage Clin.* 24, 102079. <https://doi.org/10.1016/j.nicl.2019.102079>.
- Manjon, J.V., Coupé, P., Martí-Bonmati, L., Collins, D.L., Robles, M., 2010. Adaptive non-local means denoising of MR images with spatially varying noise levels. *J. Magn. Reson. Imag.* 31 (1), 192–203.
- Miller, D.H., Barkhof, F., Frank, J.A., Parker, G.J., Thompson, A.J., 2002. Measurement of atrophy in multiple sclerosis: Pathological basis, methodological aspects and clinical relevance. *Brain* 125.
- Montalban, X., Hauser, S.L., Kappos, L., Arnold, D.L., Bar-Or, A., Comi, G., de Seze, J., Giovannoni, G., Hartung, H.P., Hemmer, B., Lublin, F., Rammohan, K.W., Selman, K., Trabulsee, A., Sauter, A., Masterman, D., Fontoura, P., Belachew, S., Garren, H., Mairon, N., Chin, P., Wolinsky, J.S., 2017. Ocrelizumab versus placebo in primary progressive multiple sclerosis. *Clin. Investigator* 376 (3), 209–220.
- Nakamura, K., Guizard, N., Fonov, V.S., Narayanan, S., Collins, D.L., Arnold, D.L., 2014. Jacobian integration method increases the statistical power to measure gray matter atrophy in multiple sclerosis. *Neuroimage Clin.* 4, 10–17. <https://doi.org/10.1016/j.nicl.2013.10.015>.
- Nakashima, I., Fujihara, K., Okita, N., Takase, S., Itoyama, Y., 1999. Clinical and MRI study of brain stem and cerebellar involvement in Japanese patients with multiple sclerosis. *J. Neurol. Neurosurg. Psychiatry* 67 (2), 153–157. <https://doi.org/10.1136/jnnp.67.2.153>.
- Ontaneda, D., Raza, P.C., Mahajan, K.R., Arnold, D.L., Dwyer, M.G., Gauthier, S.A., Greve, D.N., Harrison, D.M., Henry, R.G., Li, D.K.B., Mainero, C., Moore, W., Narayanan, S., Oh, J., Patel, R., Pelletier, D., Rauscher, A., Rooney, W.D., Sicotte, N. L., Tam, R., Reich, D.S., Azevedo, C.J., Imaging, N.A., 2021. In Multiple Sclerosis Cooperative (NAIMS), Deep grey matter injury in multiple sclerosis: A NAIMS consensus statement. *Brain* 144 (7), 1974–1984. <https://doi.org/10.1093/brain/awab132>.
- Park Aging Mind Laboratory, Dallas Lifespan Brain Study. <http://fcon.1000.projects.nitrc.org/indi/retro/dlbs.html>.
- Parmar, K., Stadelmann, C., Rocca, M.A., Langdon, D., D'Angelo, E., D'Souza, M., Burggraaf, J., Wegner, C., Sastre-Garriga, J., Barrantes-Freer, A., Dorn, J., Uitdehaag, B.M.J., Montalban, X., Wuerfel, J., Enzinger, C., Rovira, A., Tintore, M., Filippi, M., Kappos, L., Sprenger, T., 2018. MAGNIMS study group. The role of the cerebellum in multiple sclerosis - 150 years after Charcot. *Neurosci. Biobehav. Rev.* 89, 85–98. <https://doi.org/10.1016/j.neubiorev.2018.02.012>.
- Rocca, M.A., Anzalone, N., Storelli, L., Del Poggio, A., Cacciaguerra, L., Manfredi, A.A., Meani, A., Filippi, M., 2020. Deep learning on conventional magnetic resonance imaging improves the diagnosis of multiple sclerosis mimics. *Invest. Radiol.* 56 (4), 252–260. <https://doi.org/10.1097/RLI.0000000000000735>.
- Sastre-Garriga, J., Pareto, D., Battaglini, M., Rocca, M.A., Ciccarelli, O., Enzinger, C., Wuerfel, J., Sormani, M.P., Barkhof, F., Yousry, T.A., De Stefano, N., Tintore, M., Filippi, M., Gasperini, C., Kappos, L., Río, J., Frederiksen, J., Palace, J., Vrenken, H., Montalban, X., Rovira, A., 2020. MAGNIMS study group. MAGNIMS consensus recommendations on the use of brain and spinal cord atrophy measures in clinical practice. *Nat. Rev. Neurol.* 16 (3), 171–182.
- Schlaeger, R., Papinutto, N., Zhu, A.H., Lobach, I.V., Bevan, C.J., Bucci, M., Castellano, A., Gelfand, J.M., Graves, J.S., Green, A.J., Jordan, K.M., Keshavan, A., Panara, V., Stern, W.A., von Büdingen, H.C., Waubant, E., Goodin, D.S., Cree, B.A.C., Hauser, S.L., Henry, R.G., 2015. Association between thoracic spinal cord gray matter atrophy and disability in multiple sclerosis. *JAMA Neurol.* 72 (8), 897–904. <https://doi.org/10.1001/jamaneurol.2015.0993>.
- Sommer, M.A., 2003. The role of the thalamus in motor control. *Curr. Opin. Neurobiol.* 13 (6), 663–670.
- Steenwijk, M.D., Geurts, J.J., Daams, M., Tijms, B.M., Wink, A.M., Balk, L.J., Tewarie, P. K., Uitdehaag, B.M.J., Barkhof, F., Vrenken, H., Pouwels, P.J.W., 2016. Cortical atrophy patterns in multiple sclerosis are non-random and clinically relevant. *Brain* 139 (Pt 1), 115–126. <https://doi.org/10.1093/brain/awv337>.
- Tsakas, C., Magon, S., Gaetano, L., Pezold, S., Naegel, Y., Amann, M., Stippich, C., Cattin, P., Wuerfel, J., Bieri, O., Sprenger, T., Kappos, L., Parmar, K., 2019. Preferential spinal cord volume loss in primary progressive multiple sclerosis. *Mult. Scler.* 25 (7), 947–957. <https://doi.org/10.1177/1352458518775006>.

- Tustison, N.J., Avants, B.B., Cook, P.A., Zheng, Y., Egan, A., Yushkevich, P.A., Gee, J.C., 2010. N4ITK: improved N3 bias correction. *IEEE. Trans. Med. Imaging* 29 (6), 1310–1320. <https://doi.org/10.1109/TMI.2010.2046908>.
- Tustison, N.J., Holbrook, A.J., Avants, B.B., Roberts, J.M., Cook, P.A., Reagh, Z.M., Duda, J.T., Stone, J.R., Gillen, D.L., Yassa, M.A., 2019. Alzheimer's Disease Neuroimaging Initiative Longitudinal mapping of cortical thickness measurements: An Alzheimer's disease neuroimaging initiative-based evaluation study. *J. Alzheimers. Dis.* 71 (1), 165–183. <https://doi.org/10.3233/JAD-190283>.
- Vargas, D.L., Tyor, W.R., 2017. Update on disease-modifying therapies for multiple sclerosis. *J. Investig. Med.* 65 (5), 883–891.
- Vidal-Jordana, A., Sastre-Garriga, J., Perez-Miralles, F., Tur, C., Tintoré, M., Horga, A., Auger, C., Río, J., Nos, C., Edo, M.C., Arévalo, M.J., Castilló, J., Rovira, A., Montalban, X., 2013. Early brain pseudoatrophy while on natalizumab therapy is due to white matter volume changes. *Mult. Scler.* 19 (9), 1175–1181. <https://doi.org/10.1177/1352458512473190>.
- Villoslada, P., Steinman, L., 2020. New targets and therapeutics for neuroprotection, remyelination and repair in multiple sclerosis. *Expert. Opin. Investig. Drugs* 29 (5), 443–459. <https://doi.org/10.1080/13543784.2020.1757647>.
- Wolinsky, J.S., Arnold, D.L., Brochet, B., Hartung, H.P., Montalban, X., Naismith, R.T., Manfrini, M., Overell, J., Koendgen, H., Sauter, A., Bennett, I., Hubeaux, S., Kappos, L., Hauser, S.L., 2020. Long-term follow-up from the ORATORIO trial of ocrelizumab for primary progressive multiple sclerosis: A post-hoc analysis from the ongoing open-label extension of the randomised, placebo-controlled, phase 3 trial. *Lancet Neurol.* 19 (12), 998–1009. [https://doi.org/10.1016/S1474-4422\(20\)30342-2](https://doi.org/10.1016/S1474-4422(20)30342-2).
- Zivadinov, R., Bergsland, N., Dolezal, O., Hussein, S., Seidl, Z., Dwyer, M.G., Vaneckova, M., Krasensky, J., Potts, J.A., Kalincik, T., Havrdová, E., Horáková, D., 2013. Evolution of cortical and thalamus atrophy and disability progression in early relapsing-remitting MS during 5 years. *AJNR Am. J. Neuroradiol.* 34 (10), 1931–1939. <https://doi.org/10.3174/ajnr.A3503>.
- Zivadinov, R., Jakimovski, D., Gandhi, S., Ahmed, R., Dwyer, M.G., Horakova, D., Weinstock-Guttman, B., Benedict, R.R.H., Vaneckova, M., Barnett, M., Bergsland, N., 2016. Clinical relevance of brain atrophy assessment in multiple sclerosis: Implications for its use in a clinical routine. *Expert. Rev. Neurother.* 16 (7), 777–793. <https://doi.org/10.1080/14737175.2016.1181543>.
- Zivadinov, R., Reder, A.T., Filippi, M., Minagar, A., Stüve, O., Lassmann, H., Racke, M.K., Dwyer, M.G., Frohman, E.M., Khan, O., 2008. Mechanisms of action of disease-modifying agents and brain volume changes in multiple sclerosis. *Neurology* 71 (2), 136–144. <https://doi.org/10.1212/01.wnl.0000316810.01120.05>.